Supplement of Hydrol. Earth Syst. Sci., 27, 647–671, 2023
https://doi.org/10.5194/hess-27-647-2023-supplement

Hydrology and Earth System Sciences
Open Access
EGU

Supplement of

Assimilation of transformed water surface elevation to improve river discharge estimation in a continental-scale river

Menaka Revel et al.

Correspondence to: Menaka Revel (menaka@rainbow.iis.u-tokyo.ac.jp)

The supplementary materials include Text S1 to S6 and Figures S1 to S9.

S1: Amazon Basin

The Amazon River basin is a major hydrological system containing a variety of rivers, floodplains, and wetlands (Reis et al., 2019). It contains four of the world's largest rivers, namely Solimões-Amazonas, Madeira, Negro, and Japurá rivers. The Amazon Basin receives a high annual rainfall of 2,200 mm/year where 30%-40% of the rainfall is recycled locally through evapotranspiration (Fassoni-Andrade et al., 2021). The Amazon River flows into the Atlantic Ocean with an average annual discharge of $206 \times 10^3\ m^3 s^{-1}$ accounting for about 20% of total world freshwater reaching the ocean yearly (Fassoni-Andrade et al., 2021). Amazon River serves a variety of human needs, including fluvial transportation, agriculture, fishing, and energy generation. The Amazon basin has seen substantial changes in hydrological severe events such as floods and droughts in recent years, with documented increases in amplitude and frequency due to increased rainfall intensity. Furthermore, there is an obvious pattern of an increasing frequency of severe floods in the northern and main stem regions and an upward trend of extreme drought events in the southern regions (Wongchuig et al., 2019). Amazon basin have a comprehensive river observation network and very well studied especially using remote sensing (Fassoni-Andrade et al., 2021)

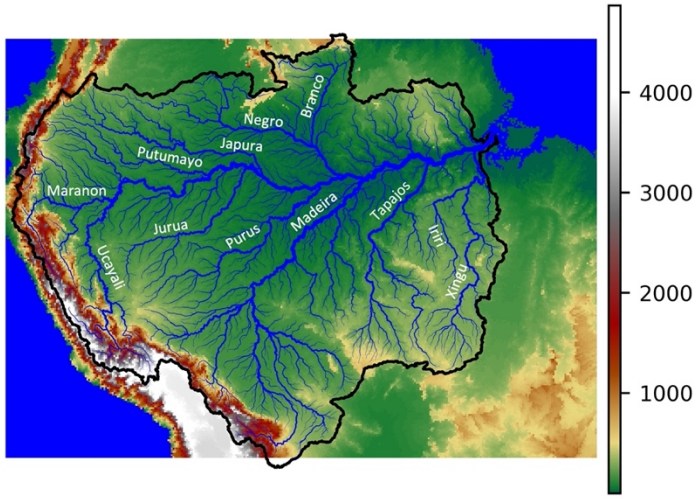

Figure S1: Amazon basin with elevations indicated by colors. River network is indicated by blue.

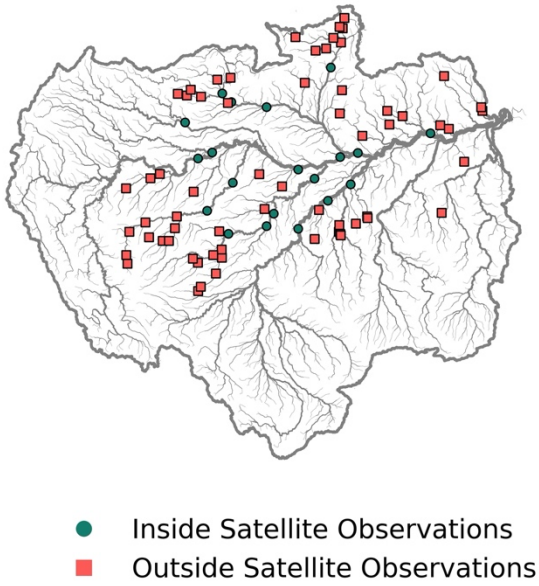

Figure S2: GRDC gauges within Satellite coverage of ENVISAT and Jason1/2 in green circles where others indicated by red squares.

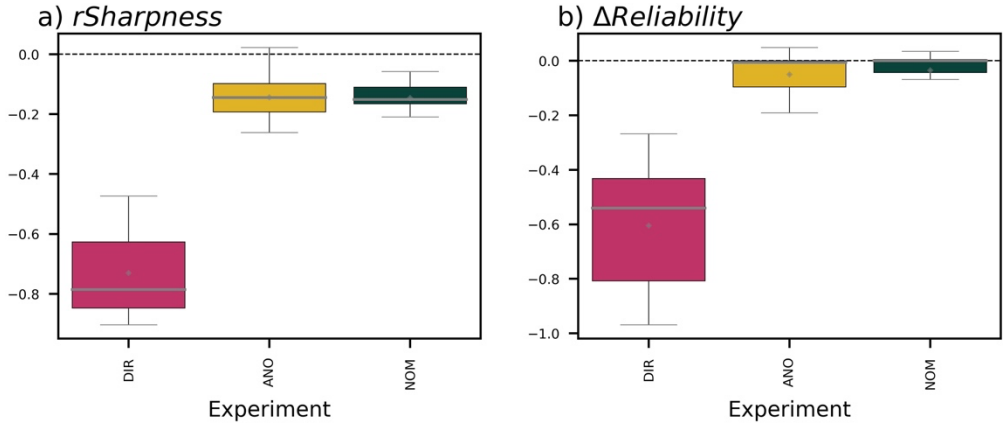

Figure S3: The boxplot of a) relative sharpness ($rsharpness$) and b) difference of reliability $\Delta Reliability$ for all the experiments. This figure indicates Exp 1 is better in reducing the confidence bound. But with the current limitations of hydrodynamic modelling reliability will become lower.

S2: Preparation of biased runoff

We introduced artificial bias into the runoff forcing data in the biased runoff experiment to determine the efficacy of DA methods when runoff is biased. We used a simple method to artificially corrupt the runoff ensemble rather than the ensemble generation method described in the main text. We generated the runoff ensemble by applying a –50% bias to the HTEESSEL (Balsamo et al., 2011) runoff product from E2O WRR2 (Dutra et al., 2017) and then perturbing it by 25% of the monthly mean runoff value. As a result of the introduction of this bias into the runoff forcing, river discharge and WSE were approximately 50% lower in the open-loop simulation results than in the observations. Figure S4 presents an example of river discharge estimation using biased runoff and GRDC observations.

S3: Preparation of corrupted bathymetry

We artificially corrupted river bathymetry by subtracting 25% of the river channel depth from the original bathymetry to investigate the efficacy of DA when river bathymetry is erroneous. Basically, this process deepened the river channel, lowering

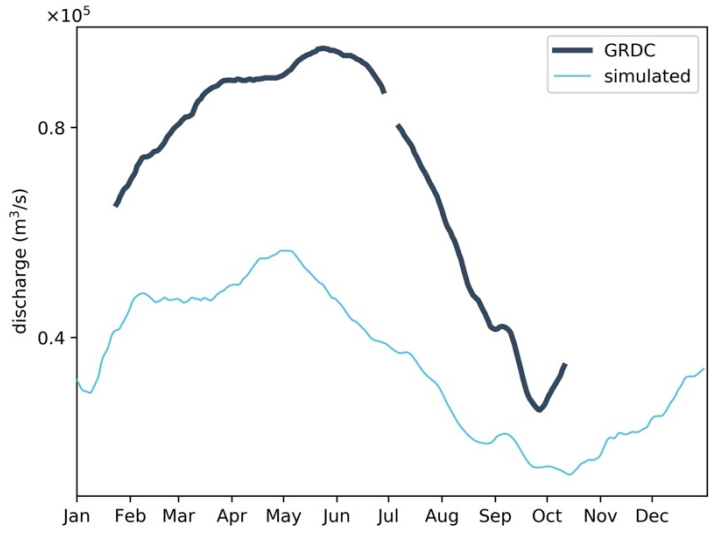

Figure S4: River discharge comparison between observation (GRDC) and discharge simulated by biased runoff of HETESSEL E2O WRR2.

the river bathymetry. The original river channel depth was calculated with a power-law equation (Yamazaki *et al*., 2011; Zhou *et al*., 2022),

$$\boldsymbol{B = max\left(B_{min}, c_B Q_{avg}^{p_B}\right)} \quad (1)$$

where B is the channel depth (m) and Q_{avg} is the annual average discharge (m^3/s). Here, the average climatological land surface runoff from the Minimal Advanced Treatment of Surface Interaction Runoff (MATSIRO; Takata *et al*., 2003), simulated by Kim *et al*. (2009), was used. Other parameters were estimated to be $B_{min} = 1.0$, $c_B = 0.1$, and $p_B = 0.5$. Figure S4 shows the difference in river channel depth between the corrupted and original values.

S4: Data assimilation into a calibrated hydrodynamic model

The hydraulic parameters were used to transfer the corrections to the next time step in DA. Therefore, we compared the river bottom–calibrated model with the conventional CaMa-Flood model to understand the impact of river bathymetry calibration on various DA techniques. We chose to calibrate the river channel bathymetry because uncertainty in river bathymetry is one of the largest sources of error in hydrodynamic modeling (Brêda *et al*., 2019). Inaccuracy in river bathymetry strongly affected the WSE and worsened the model's performance compared to satellite altimetry measurements. River bathymetry was calibrated with the rating curve method (i.e., the discharge–WSE relationship; Zhou *et al*., 2022). Calibration was performed with *in situ* river discharge observations and satellite altimetry. The calibrated model simulated WSE more precisely than uncalibrated methods relative to WSE observations, but this calibration method did not drastically improve river discharge.

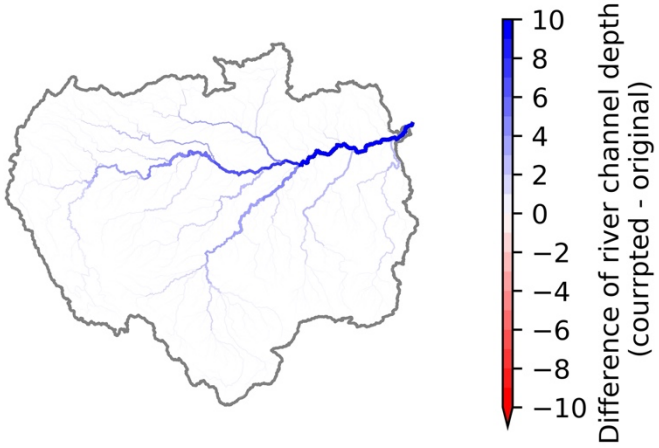

Figure S5: Difference of river channel depth between corrupted and original bathymetry.

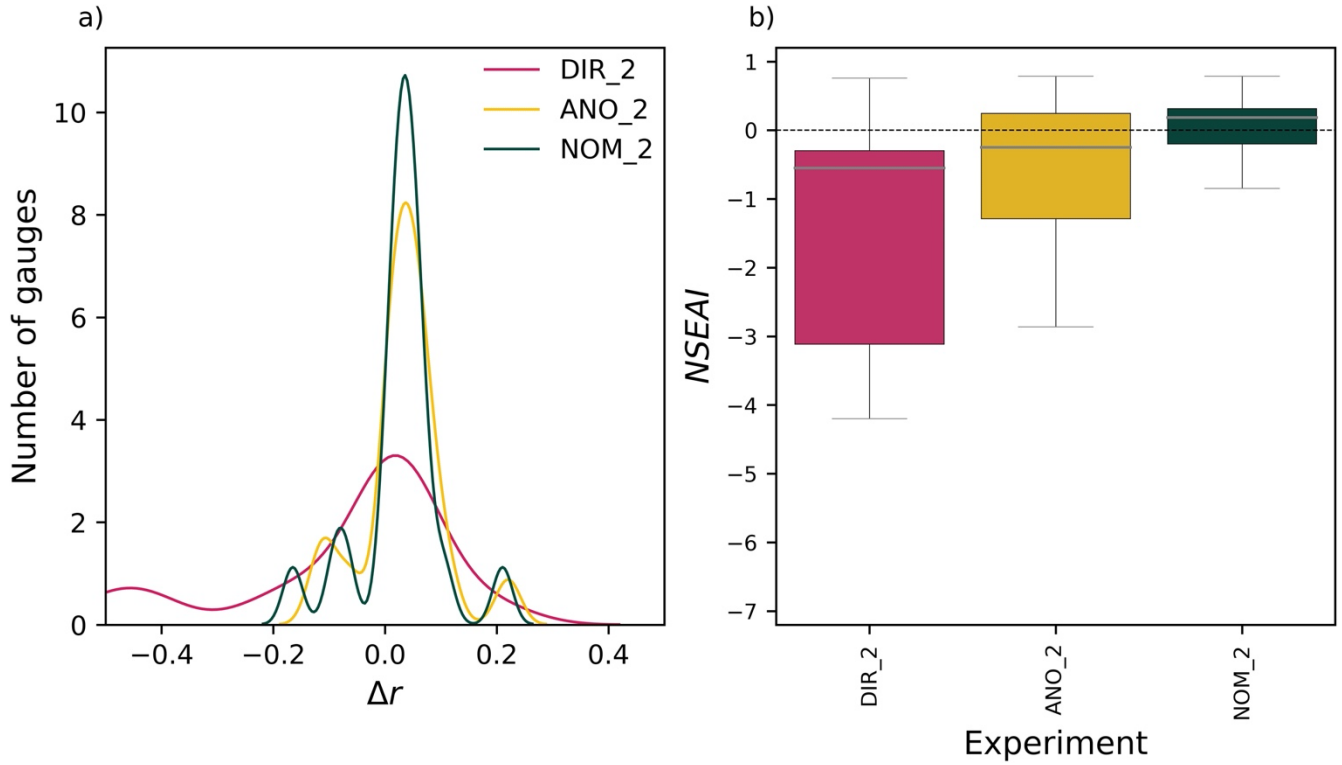

Figure S6: a) Probability distribution of the correlation coefficient (Δr) for each experiment, shown in blue, yellow, and red for direct (DIR_2), anomaly (ANO_2), and normalized value (NOM_2) using calibrated model, respectively. b) Boxplots of the Nash-Sutcliffe based assimilation index ($NSEAI$) of assimilated compared to open-loop discharge for all the experiments. Boxes in blue, yellow, and red indicates direct (DIR_2), anomaly (ANO_2), and normalized value (NOM_2) using calibrated model, respectively.

More information about the methods used to calibrate river channel bathymetry can be found in Zhou *et al*. (2022). Hereafter, "calibrated model" refers to the CaMa-Flood model in which the river channel bathymetry was calibrated using the rating curve method. We denote the direct, anomaly, and normalized value DA experiments as DIR_2, ANO_2, and NOM_2, respectively.

Figure S6a illustrates the kernel density estimate of the probability density function for the Δr of river discharge. All experiments that used the calibrated model (i.e., DIR_2, ANO_2, and NOM_2) showed an improvement in median Δr (> 0), which indicates improved simulation of the flow regimes with DA for 50% or more of all gauges. The Δr of river discharge in DIR_2 showed a left-skewed distribution, which suggests poor reconstruction of seasonality at some gauges (47.6%). At a few locations, the flow regimes improved greatly ($\Delta r > 0.2$) with calibration of the river bathymetry. More than 70% of gauges showed flow regime improvements in the anomaly and normalized value DA experiments. However, Exp 3a had positive median $NSEAI$ values, which indicates that at least 50% of gauges had improved NSE values with DA. Figure S6b shows a boxplot of $NSEAI$ for all experiments, indicating considerable improvement in the DA experiments with normalized value assimilation.

S5: Data assimilation under various conditions

We compared the DA performances with different hydrodynamic model conditions and combinations of them. We tested biased runoff condition ("with runoff bias": Text S2); corrupted bathymetry condition ("with bathymetry error": Text S3); and a combination of biased runoff and corrupted bathymetry. Figure S7 indicates the hydrograph of Mancapuru gauging station for different DA methods and different model conditions. The normalized assimilation method estimated the discharge closer to the observed discharge neither with any runoff bias nor bathymetry error. But when the bathymetry error is imposed none

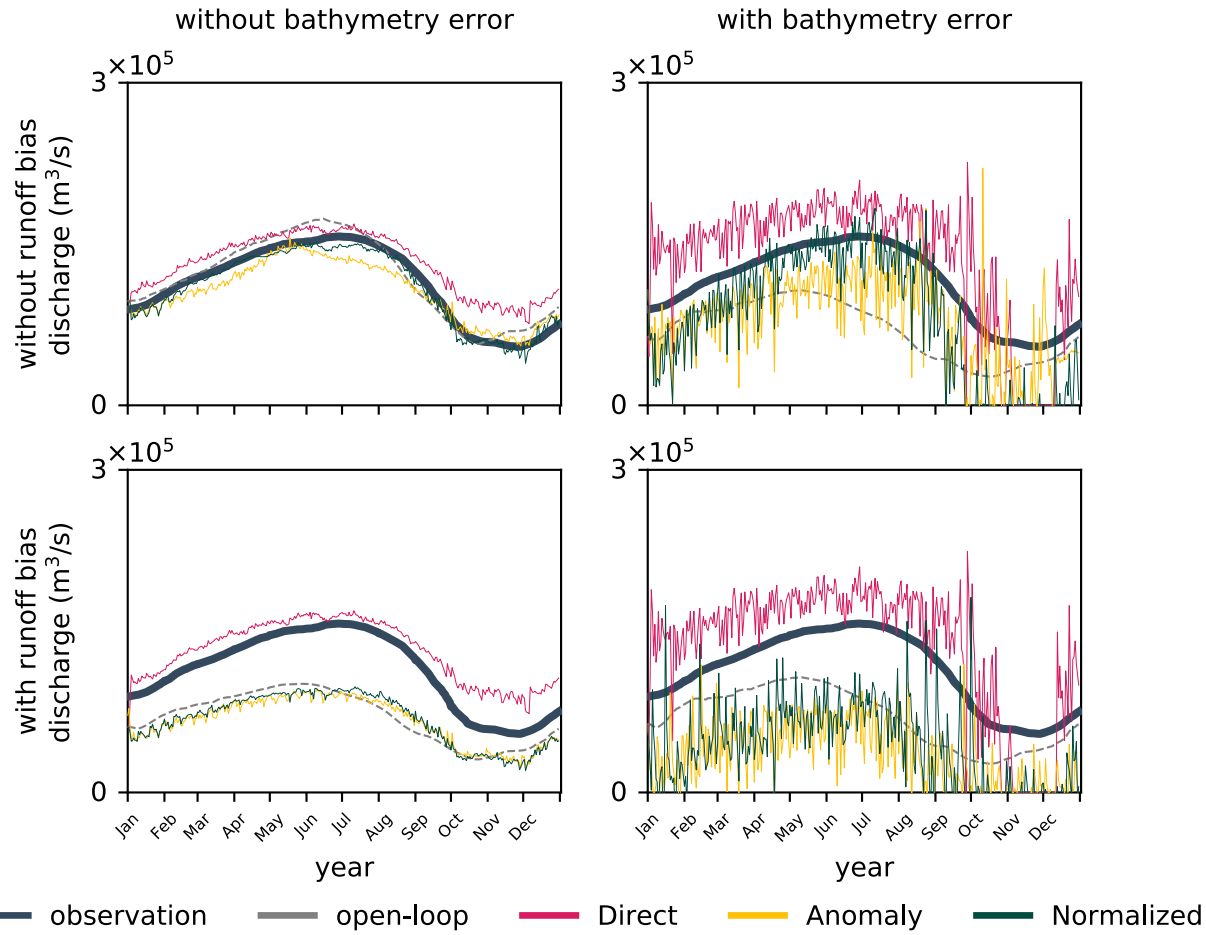

Figure S7: Hydrographs of assimilated river discharge under various conditions: a) without runoff bias or bathymetry error, b) without runoff bias and with bathymetry error, c) with runoff bias and without bathymetry error, and d) with runoff bias and bathymetry error. The direct, anomaly, and normalized value DA results are represented in blue, yellow, and red, respectively.

of the assimilation methods performed better than the open-loop simulation. When the runoff was erroneous the direct DA method performed better in estimating river discharge. The main reason for poor performance in anomaly and normalized value DA methods especially in bathymetry error conditions is the underestimation of the open-loop statistics (i.e., mean and standard deviation). The better performance of direct DA with runoff bias and without bathymetry error can be due to no error in river channel parameters (i.e., river bathymetry). Therefore, the poor performance of the anomaly and normalized value DA methods is due to the errors in the statistics used to generate anomalies and normalized values in the erroneous hydrodynamic model.

S6: Annual peak and though estimation

We investigated further into the peak and low flow values of the normalized value assimilation experiments namely normalized value assimilation with normal conditions (NOM) and normalized assimilation to calibrated model (NOM_2); since they are important parameters of a hydrograph that directly affects floods and drought occurrences. Normalized assimilation underestimated annual maximum discharges while accurately estimating annual low flows (Figure S9). Peak discharge underestimation is noticeable in larger river segments, such as the Amazon mainstem. Other limitations of global hydrodynamic modeling, such as the uncertainties of river width estimations, the assumption of rectangular river cross-sections and simplified floodplain physics, might contribute to these underestimations. Improving the parameters directly involved in converting assimilated WSE values to prognostic variables in the model is important for a successful assimilation framework.

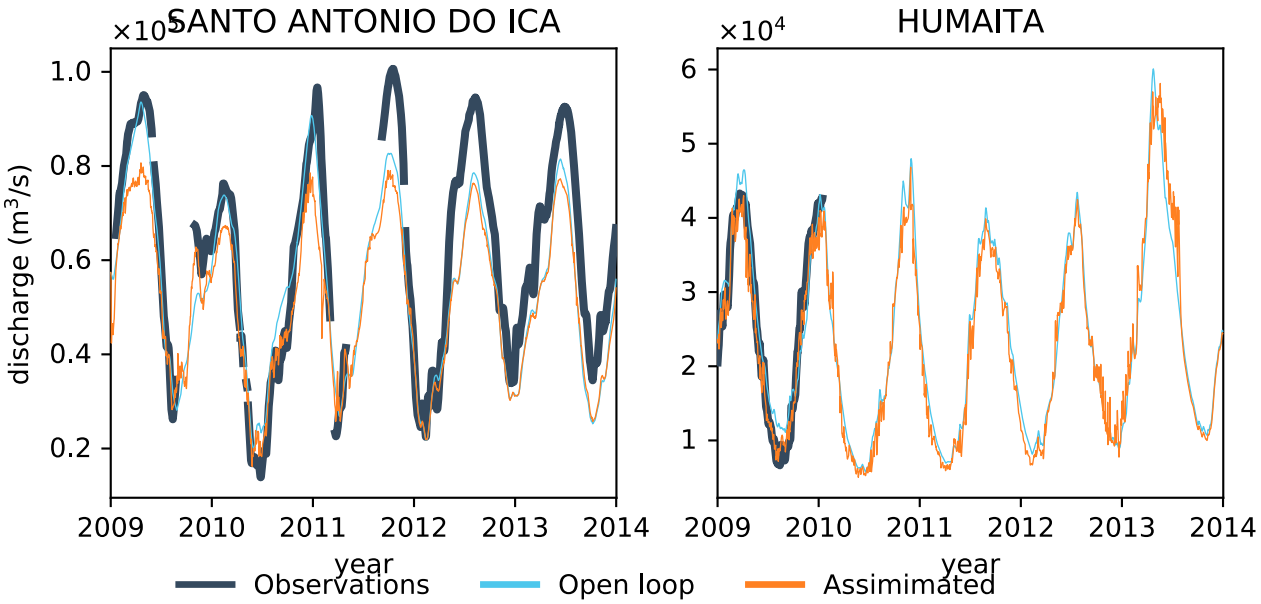

Figure S8: Hydrographs for Santo Antonio Do ICA, and Humaita in Amazon and Maderia rivers, respectively. Observations, open loop, and assimilated river discharge presented in black, blue, and orange. Santo Antonio Do ICA represents the ability of DA to characterise the unexpected secondary peak. Humaita hydrograph shows the DAs' ability to estimate low flows better.

85

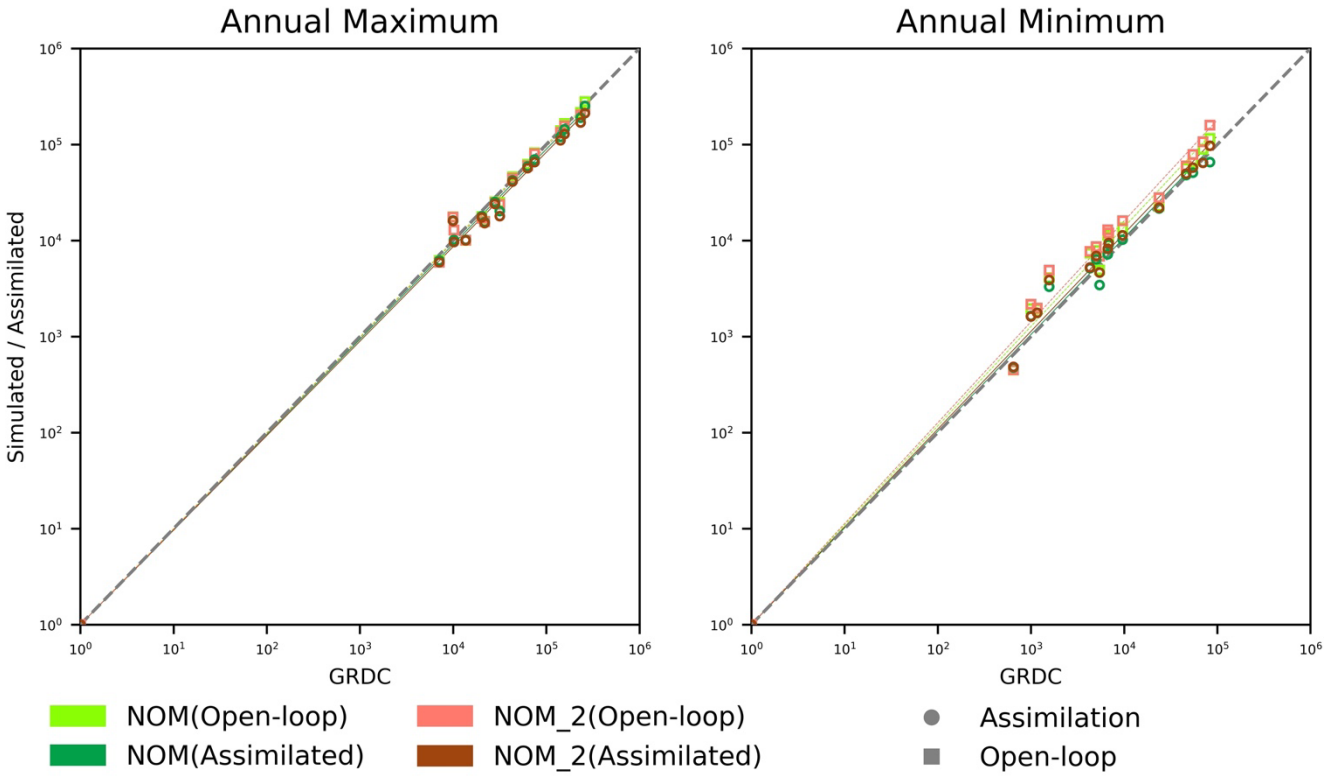

Figure S9: Scatter plot of the simulated annual maximum and minimum compared to observed maximum river discharge for NOM and NOM_2. Circles and squares represents assimilated and open-loop river discharge, respectively.

Reference:

Balsamo, G., Dutra, E., Beljaars, A. and Viterbo, P.: Evolution of land-surface processes in the IFS, ECMWF Newsl.,

127(January), 6, doi:10.21957/x1j3i7bz, 2011.

Brêda, J. P. L. F., Paiva, R. C. D., Bravo, J. M., Passaia, O. A. and Moreira, D. M.: Assimilation of Satellite Altimetry Data for Effective River Bathymetry, Water Resour. Res., 55(9), 7441–7463, doi:10.1029/2018WR024010, 2019.

Dutra, E., Gianpaolo, B., Jean-Christophe, C., Munier, S., Burke, S., Fink, G., Van Dijk, A., Martinez-de la Torre, A., van Beek, R., De Roo, A. and Polcher, J.: Report on the improved water resources reanalysis Deliverable. [online] Available from: http://earth2observe.eu/files/Public Deliverables/D5.2 - Report on the Improved Water Resources Reanalysis (WRR tier 2).pdf, 2017.

Fassoni-Andrade, A. C., Fleischmann, A. S., Papa, F., Paiva, R. C. D. de, Wongchuig, S., Melack, J. M., Moreira, A. A., Paris, A., Ruhoff, A., Barbosa, C., Maciel, D. A., Novo, E., Durand, F., Frappart, F., Aires, F., Abrahão, G. M., Ferreira-Ferreira, J., Espinoza, J. C., Laipelt, L., Costa, M. H., Espinoza-Villar, R., Calmant, S. and Pellet, V.: Amazon Hydrology From Space: Scientific Advances and Future Challenges, Rev. Geophys., 59(4), 1–97, doi:10.1029/2020RG000728, 2021.

Kim, H., Yeh, P. J. F., Oki, T. and Kanae, S.: Role of rivers in the seasonal variations of terrestrial water storage over global basins, Geophys. Res. Lett., 36(17), 2–6, doi:10.1029/2009GL039006, 2009.

Reis, V., Hermoso, V., Hamilton, S. K., Bunn, S. E., Fluet-Chouinard, E., Venables, B. and Linke, S.: Characterizing seasonal dynamics of Amazonian wetlands for conservation and decision making, Aquat. Conserv. Mar. Freshw. Ecosyst., 29(7), 1073–1082, doi:10.1002/aqc.3051, 2019.

Takata, K., Emori, S. and Watanabe, T.: Development of the minimal advanced treatments of surface interaction and runoff, Glob. Planet. Change, 38(1–2), 209–222, doi:10.1016/S0921-8181(03)00030-4, 2003.

Wongchuig, S. C., de Paiva, R. C. D., Siqueira, V. and Collischonn, W.: Hydrological reanalysis across the 20th century: A case study of the Amazon Basin, J. Hydrol., 570(November 2018), 755–773, doi:10.1016/j.jhydrol.2019.01.025, 2019.

Yamazaki, D., Kanae, S., Kim, H. and Oki, T.: A physically based description of floodplain inundation dynamics in a global river routing model, Water Resour. Res., 47(4), 1–21, doi:10.1029/2010WR009726, 2011.

Zhou, X., Revel, M., Modi, P., Shiozawa, T. and Yamazaki, D.: Correction of river bathymetry parameters using the stage-discharge rating curve, Water Resour. Res., 1–26, doi:10.1029/2021WR031226, 2022.